Where large deep-ocean waves break

Hans van Haren, Andrea Cimatoribus, Louis Gostiaux

AGU PUBLICATIONS

Geophysical Research Letters

RESEARCH LETTER
10.1002/2015GL063329

Key Points:
- Large turbulence variability is observed over a short slope range
- Different turbulence structures are demonstrated in detail
- Large internal wave breaking and small-scale layering are key features

Correspondence to:
H. van Haren,
hans.van.haren@nioz.nl

Citation:
van Haren, H., A. Cimatoribus, and L. Gostiaux (2015), Where large deep-ocean waves break, *Geophys. Res. Lett.*, *42*, 2351–2357, doi:10.1002/2015GL063329.

Received 31 JAN 2015
Accepted 5 MAR 2015
Accepted article online 27 MAR 2015
Published online 3 APR 2015

Where large deep-ocean waves break

Hans van Haren[1], Andrea Cimatoribus[1], and Louis Gostiaux[2]

[1]Royal Netherlands Institute for Sea Research, Den Burg, Netherlands, [2]Laboratoire de Mécanique des Fluides et d'Acoustique, UMR CNRS 5509, École Centrale de Lyon, Université de Lyon, Écully, France

Abstract Underwater topography like seamounts causes the breaking of large "internal waves" with associated turbulent mixing strongly affecting the redistribution of sediment. Here ocean turbulence is characterized and quantified in the lowest 100 m of the water column at three nearby sites above the slope of a deep-ocean seamount. Moored high-resolution temperature sensors show very different turbulence generation mechanisms over 3 and 5 km horizontal separation distances. At the steepest slope, turbulence was 100 times more energetic than at the shallowest slope where turbulence was still 10 times more energetic than found in the open ocean, away from topography. The turbulence on this extensive slope is caused by slope steepness and nonlinear wave evolution, but not by bottom-friction, "critical" internal tide reflection or lee wave generation.

1. Introduction

The maintenance of the stable vertical density stratification in the ocean [*Munk and Wunsch*, 1998], the redistribution of sediment from the seafloor and the replenishment of near-surface nutrients, necessary for plankton growth, have in common that they depend on mechanical diapycnal turbulent mixing. This common dependence does not imply that turbulent mixing is evenly distributed through the ocean. As a function of time and space, vertical turbulent diffusivity can reach up to 10^6 times the molecular diffusivity [e.g., *Gregg*, 1989]. Thus, we are investigating areas and processes that contribute most to ocean mixing. As the prominent mixing process is suggested to be the breaking of "internal waves" [*Orlanski and Bryan*, 1969], we particularly study those areas and processes that cause smooth sinusoidal waves to steepen and overturn (break). New results of one such search are presented here, using detailed deep-ocean observations.

Internal gravity waves can freely propagate in three dimensions through the ocean interior when they have a frequency between inertial f (due to the rotation of the Earth) and buoyancy N (due to the vertical density stratification). Their wave periods consequently vary between several minutes and 1 day and generally include semidiurnal tides, a dominant internal wave source. Mixing due to internal wave breaking is suggested [*Eriksen*, 1982; *Thorpe*, 1987] to mainly occur in the vicinity of underwater topography, in addition to turbulent bottom-friction processes [*Armi*, 1979; *Garrett*, 1990]. However, the latter processes create a near-homogeneous bottom boundary in which the mixing efficiency tends to become low. In contrast, internal wave breaking re-organizes stratification in thin layers [*Thorpe*, 1988]. The thin layers are transported to within a few meters of the seafloor [*van Haren*, 2005]. Both processes contribute to efficient mixing.

Since "critical" bottom slopes, matching the slope of internal wave beams that depends on wave frequency and f and N, concentrate the reflected wave energy following linear theory, largest wave breaking was expected at such slopes [*Klymak et al.,* 2008, 2010]. However, although some sedimentological observations [*Cacchione and Drake*, 1986; *Dickson and McCave*, 1986; *van Raaphorst et al.*, 2001] suggest evidence of enhanced wave breaking at slopes that match the tidal wave slope, no detailed observations have confirmed such preferential breaking. Instead, strong internal wave breaking has also been observed at noncritical slopes [*van Haren*, 2005], at the foot of a continental slope [*Bonnin et al.*, 2006; *Nash et al.*, 2007], and in areas where the main generation process is "subinertial," with frequencies $\sigma < f$ [*Thorpe*, 1987; *Hosegood et al.*, 2004]. These observations partially confirm theoretical suggestions [*Thorpe*, 1988] that nonlinear interaction occurs between incoming and reflecting internal waves above subcritical (shallow) slopes. We are thus still in search for conditions causing such large internal waves to break and which dominate sediment redistribution and ocean mixing on a global scale.

In this paper, we present estimates of turbulence intensities with large variations over short horizontal distances (in oceanographic context) of 3 and 5 km. Turbulence is studied here over ranges between 1 and 10^4 s in time and between 1 and 100 m in the vertical. The estimates are made using high-resolution

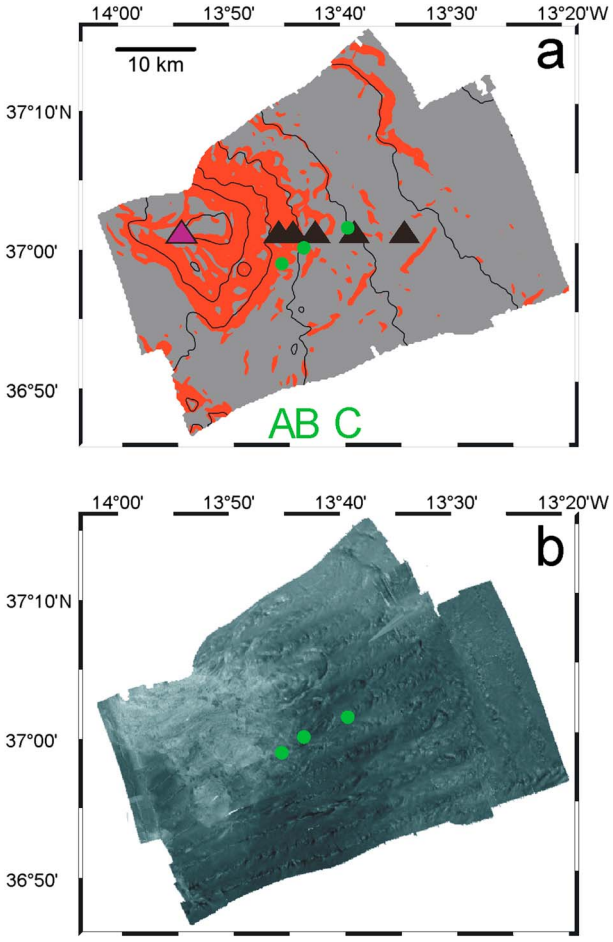

Figure 1. Monte Josephine topography. (a) Smoothed 250 × 250 m grid Multibeam data. Mooring sites A–C are indicated by green circles, conductivity-temperature-depth (CTD) stations by triangles. Solid black contours indicate water depth every 500 m, red indicates semidiurnal lunar tidal supercritical bottom slopes ($\gamma > 5.7°$), and grey subcritical ($\gamma < 5.7°$). (b) Backscatter strength (high values = light shading: coarse grain sizes and/or compacted sediment; low = dark: fine grain sizes and/or water-rich sediment).

observations from self-contained temperature sensors; details of the data handling are given in the appendix. These sensors are moored 3 times for several months at different sites on the northeasternmost slopes (Figure 1) of underwater seamount Monte Josephine in the NE Atlantic Ocean, 450 km southwest of Lisbon, Portugal. This volcano complex, probably the epicenter of the 1755 Lisbon earthquake and tsunami, rises from the 5000 m deep ocean floor to just under 250 m from the surface, with a diameter of roughly 100 km.

2. Observations

Monte Josephine consists of several subsummits. The subsummit with mooring sites extends up to 800 m below the surface. The sites' bottom slope varies by a factor of 3 and from supercritical to subcritical for the dominant semidiurnal tide (Figure 1a). The sites are well below (1400, 1700, and 2100 m) and more than 10 km horizontally from the subsummit, to avoid the measuring of nonlinear, potentially breaking internal waves caused by hydraulic jumps associated with arrested lee waves by the flow over sharp topography [*Klymak et al.*, 2010]. As the main local internal tide generation is near the (sub)summit, the sites are all below the main tidal beam [*Gonella and Michon*, 1988], which appears to be patchy in spatial energy distribution [*van Haren et al.*, 2010]. The sites are also deeper than 1500 m, below the Mediterranean outflow in the Atlantic to avoid any influence of salinity-compensated temperature inversions, as salinity is not measured.

Mooring sites (named "A, B, and C") configuration, duration, and slope are in Table 1. The local bottom slope γ was computed from $|dz/dx, dz/dy|$ using original 30 × 60 m horizontal resolution Multibeam data smoothed onto a 250 × 250 m grid. At 2530 m ("B"), $\gamma = 5.7°$ and was critical for the internal tide as its beam slope $\beta = \sin^{-1}((\sigma^2 - f^2)^{1/2}/(N^2 - f^2)^{1/2}) = 5.7 \pm 1°$ for $\sigma = M_2$ the semidiurnal lunar tidal frequency and N computed from observations at 2500 m. At 2210 m ("A"), γ is supercritical $\beta \approx 0.4\gamma$. At 2937 m ("C"), γ is subcritical $\beta \approx 2.3\gamma$.

From Table 1 we see that 4 days and 100 m mean turbulence dissipation rates [$<\varepsilon>$] do not vary by a factor of more than 4 for any site (in the appendix details are given how turbulence estimates were made). This is an indication that turbulence is only weakly modulated by time-dependent processes like mesoscale eddies. A small error in the estimates is obtained (Figure 2, green circles that include the error bars) thanks to the low noise level and high sampling rate of the temperature sensors. Between the sites, however, the mean values vary strongly and significantly: $[<\varepsilon>] = O(10^{-7})$, via $O(10^{-8})$ to $O(10^{-9})$ W kg^{-1} (Table 1), as a function of

Table 1. Turbulence Parameter Estimates Averaged Over Entire Time Series (Except for 2530 m Data) and Over Arbitrary 4 days of Temperature Observations Computed for the Three Consecutively Occupied Mooring Sites, and Averaged Over the Lower 100 m[a]

Latitude	Longitude	Water Depth (m)/Slope γ (°)	#Sensors/Interval (m)/First (mab)	Averaging Period (yd)	$[<\varepsilon>]$ (W kg^{-1})	$[<K_z>]$ (m^2 s^{-1})	$[<N>]$ (s^{-1})
A: 36°59′N	13°45′W	2210/9.4	144/0.7/5	103–224	2.4×10^{-7}	2.4×10^{-2}	1.4×10^{-3}
				198–202	8.6×10^{-8}	1.2×10^{-2}	1.4×10^{-3}
				205–209	3.3×10^{-7}	2.5×10^{-2}	1.7×10^{-3}
B: 37°00′N	13°43′W	2530/5.7	140/0.6,1.0/7	306(–365)−103	–	–	–
				307–310	2.4×10^{-8}	7.8×10^{-3}	1.1×10^{-3}
				310–314	2.4×10^{-8}	6.0×10^{-3}	1.0×10^{-3}
C: 37°01′N	13°39′W	2937/3.2	140/1.0/5	224–290	2.8×10^{-9}	2.4×10^{-3}	6.9×10^{-4}
				234–238	3.3×10^{-9}	3.1×10^{-3}	6.4×10^{-4}
				238–242	1.9×10^{-9}	1.8×10^{-3}	7.0×10^{-4}

[a](mab = meters above bottom; yd = yearday 2013).

decreasing slope from semidiurnal tidally supercritical (A), via critical (B), to subcritical (C). Such high significance cannot be obtained in estimates from CTD profiles along 37°01′N, averaged over the lower 400 m (Figure 2, triangles). In spite of the large error, these turbulence parameter estimates roughly confirm the detailed mooring observations, see especially site C where a CTD was taken close to the mooring. The observed variation in mean dissipation rate follows the order from light to dark representing decreasing sediment size and surface reflectance in Multibeam data (Figure 1b). This indicates sediment size and compacting increase as turbulence and currents increase, suggesting all the fine sediment is resuspended and flushed away.

The observed variation by 2 orders of magnitude in mean turbulence over a modest change in cross-slope distance and depth was not foreseen after first viewing the original temperature data. Taking from each mooring four sample days, Figures 3a–5a for sites A–C, we observe the semidiurnal tidal periodicity in all. With increasing depth, the temperature range varies from 1.0, via 0.4 to 0.15°C, but tidal current amplitude and mean buoyancy frequency vary only by a factor of 2.3 in total, while the internal tidal amplitude is about the same: 100 m (trough-crest).

The large variation between the sites is in the observed turbulent displacements of water parcels from their statically stable positions (for definitions, see the Appendix), Figures 3b–5b. At site A, the displacements exceed 90 m, at least once a tidal cycle from the lowest sensor at 5 m above the bottom, and occur much more often than at deeper sites. The few tens of meters high displacements at site B seldom reach the lowest sensor. The even smaller displacements at site C never do so. Locally, time series of 100 m vertical averages of turbulence

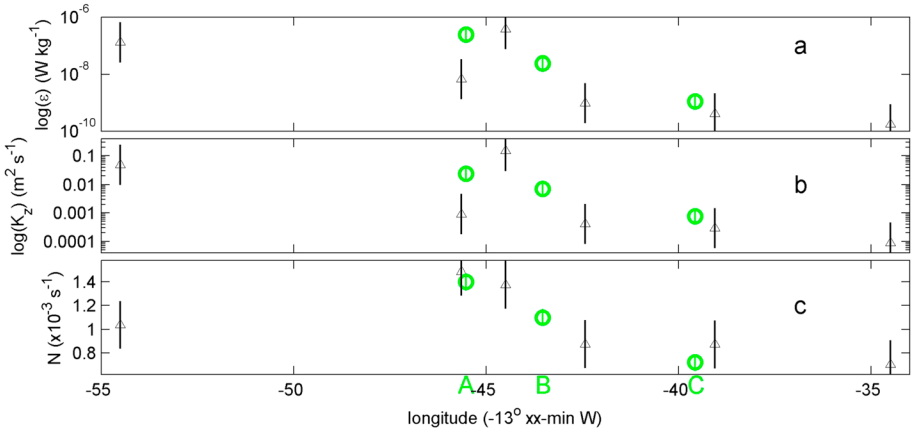

Figure 2. Cross-slope transect of average turbulence parameters along 37°01′N. (a) Turbulence dissipation rate. (b) Turbulent diffusivity. (c) Buoyancy frequency. 4 day/100 mab (m above the bottom) mean estimates from moored temperature data (green circles) are compared with 30–400 m above the bottom average estimates from single CTD profile data (triangles), all >2000 m water depth, except for the leftmost one (1100 m). Note that the moored data error bars (vertical lines) are thus small that they fall entirely within the green circles.

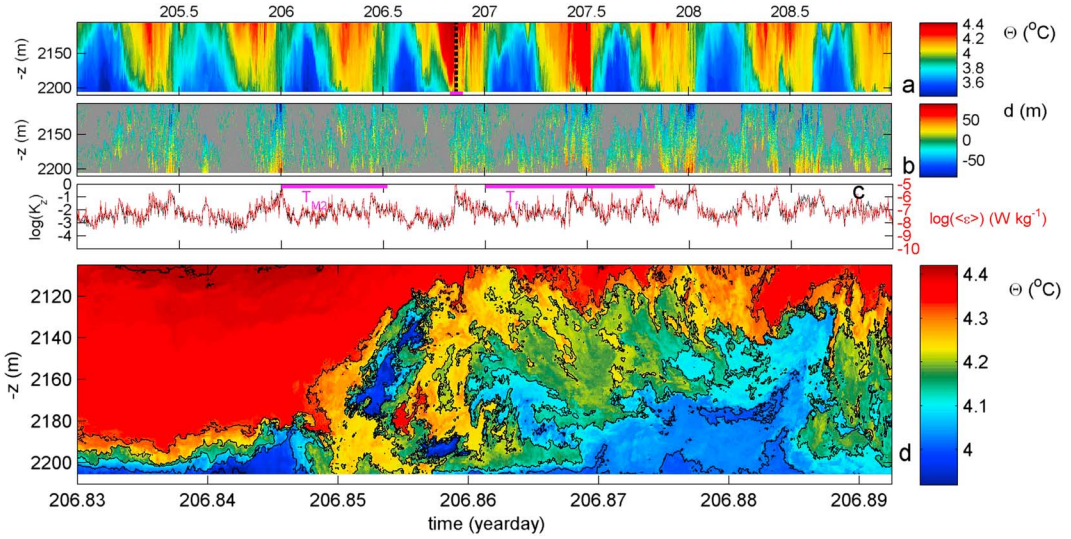

Figure 3. Four days of internal wave motions and turbulence observed at site A. (a) Depth-time series of conservative temperature. The black dashed line indicates the period in Figure 3d. (b) Turbulent displacements computed after sorting data in Figure 3a to stable profiles every time step. (c) Time series of logarithm of vertically averaged dissipation rate and diffusivity. Purple bars indicate semidiurnal tidal "T_{M2}" and inertial "T_f" periods. (d) One-and-a-half-hour sample detail of Figure 3a, with solid black contours every 0.1°C.

parameters show variations of 2–3 orders of magnitude over periods smaller than $2\pi/N = T_N \approx 1.3$–3 h (A–C), Figures 3c–5c. A clear variation with tidal phase is not observed, but at site A the largest peak occurs at the transition between downslope and upslope phase, while at site B a distinct fourth diurnal periodicity is observed.

The associated turbulence processes are characterized in Figures 3d–5d on a time range of about one buoyancy period T_N long so that all motions varying as a function of time represent turbulent motions, which have periods smaller than T_N, and not freely propagating waves, which have periods larger than T_N. At site A, intense turbulence occurs in brief periods at the end of the downslope phase when relatively cold water starts moving upslope, as in a frontal bore, Figure 3d: the arrival of a highly nonlinear internal wave breaking. Only such wave breaking is capable of resuspending sediment and distributing it tens of meters away from the seafloor within minutes [*Hosegood et al.*, 2004]. At site B, large overturns are more often observed during

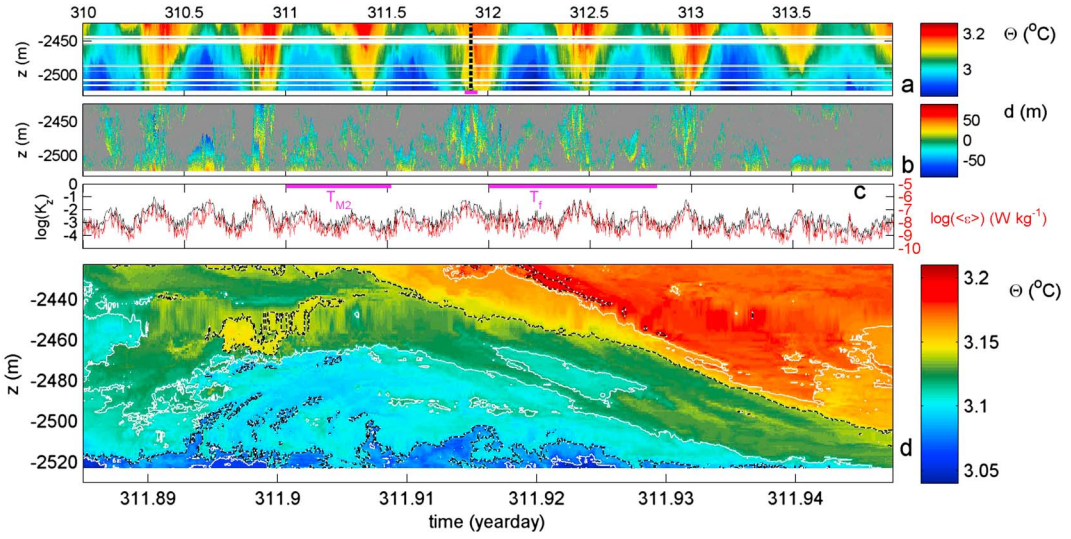

Figure 4. As Figure 3, but for site B. (a) Missing sensor data are indicated by horizontal bands. These are linearly interpolated for further analysis. (d) Dashed black contours are drawn every 0.05°C, solid white every 0.025°C. Note change in color scales for Figures 4a and 4d.

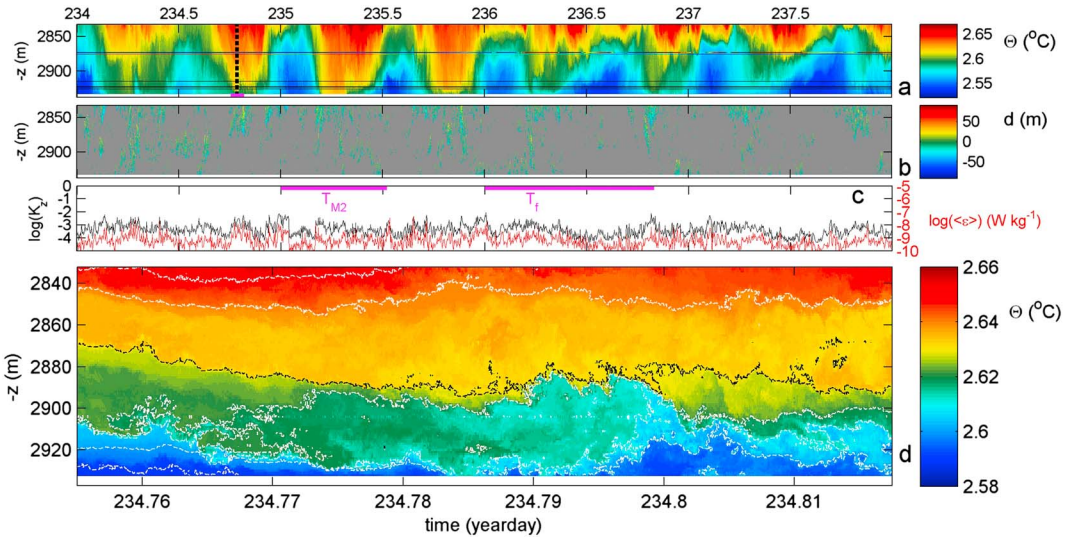

Figure 5. As Figure 4, but for site C. (d) Dashed black contours are drawn every 0.05°C, dashed white every 0.01°C. Note change in color scales for Figures 5a and 5d.

the warming downslope phase of the tide, Figure 4d. During this phase, showing a portion of the downslope moving internal wave, the vertical current difference (shear) across the vertical temperature gradient is generated by a downslope motion in the upper, warm layer and upslope motion in the lower, cold layer. A secondary, convectively driven turbulence peak occurs around maximum cool period (Figures 4a and 4b). At site C, interfaces are even more horizontal, Figure 5d. Quasi-permanent small-scale turbulence is found in weak stratification, "concentrated" between thin layering that is mainly horizontal.

3. Discussion

Evidence for the coexistence of different turbulence generation mechanisms (convection and shear) at sites separated by short distances is provided by moored high-resolution temperature observations. A strong decrease is found in turbulence dissipation rate down a deep concave slope varying from steep to shallow over a relatively short vertical (<700 m) and horizontal (<10 km) distance. Comparable variations in turbulence intensity have been reported [*Nikurashin and Legg*, 2011; *Iwamae and Hibiya*, 2012] for 2-D computer model results simulating a confined flow in a deep channel. Other numerical simulations over 100 m topography scales [*Legg and Adcroft*, 2003] suggest that mixing occurs over the lower (subcritical) part of a concave slope mainly. We argue that the present precise ocean observations are relevant for the more general case of internal wave breaking over sloping topography in a full 3-D context.

At the distinct site of critical semidiurnal tidal slope around 2500 m, no obvious enhanced turbulence process is found. We speculate a cause by nonuniform stratification. Instead, at steeper, supercritical slopes highly nonlinear upslope moving bores and vigorous turbulence are found. Apparently there, the dominant wave phase speed matches the particle velocity so that waves steepen and break. Above Monte Josephine, such turbulence processes cannot be associated with bottom friction as the [0.05–0.12] m s^{-1} weak currents cause an (Ekman) boundary layer of less than 5 m [*Ekman*, 1905] confirming theoretical considerations on the effects of nonlinear internal wave breaking [*Thorpe*, 1988]. The observed turbulence cannot also be associated with an internal hydraulic jump or an arrested lee wave, which extend at most several 100 m [*Klymak et al.*, 2010] but not 1400 m vertically below the subsummit. The turbulence diffusivity $K_b = 2 \times 10^{-2}$ m^2 s^{-1}, the K_z value over the "bottom boundary" height h, in this case the measured portion of the water column, is 1000 times larger than open-ocean values and 200 times the interior mean K_z value $K_{req} = 10^{-4}$ m^2 s^{-1} required to maintain the deep-ocean stratification [*Munk*, 1966; *Munk and Wunsch*, 1998]. As a result, in terms of $K_{req} = K_b \cdot S_b(z,h)/S(z)$, where $S(z)$ denotes the horizontal surface area at depth z and $S_b(z,h)$ the part of $S(z)$ that would be lying within a boundary layer of thickness h, a relatively narrow range of about 450 m in depth interval, about one seventh of the depth range, would generate sufficient mixing for the entire deep ocean

[*Armi*, 1979; *Garrett*, 1990], assuming ubiquitous internal waves, a 3000 m average ocean depth, a $h = 100$ m thick turbulent layer [*Eriksen*, 1982] (present observations), so that $S/S_b = 30 \approx 1/7 \cdot K_b/K_{\mathrm{req}}$ as observed.

Appendix A: Data and Methods

The taut-wire moorings contained at least 100 "NIOZ4" temperature sensors. NIOZ4 is an upgrade of "NIOZ3" [*van Haren et al.*, 2009], with similar characteristics (precision $<5 \times 10^{-4}$°C and a noise level of 6×10^{-5}°C). A single elliptic buoy provided 3000 N net buoyancy, ensuring small mooring motions of <0.1 m in the vertical and <5 m in the horizontal as verified using tilt and pressure sensor data. Sampling rate was 1 Hz. All temperature sensors were synchronized via induction every 4 h, so that timing mismatch was <0.02 s. Some showed battery problems and 15 sensors were lost during one unfortunate recovery. Large-scale currents were sampled acoustically, once every 15 min.

The moored observations are supported by shipborne observations during deployment/recovery cruises. A Kongsberg EM302 30 kHz Multibeam was used for extensive high-resolution bathymetry mapping. From its backscatter strength data, relative variations in grain size and sediment compacting are estimated. SeaBird 911-plus conductivity-temperature-depth (CTD) profiles were made for larger-scale hydrographic survey and calibration purposes including turbulence parameter estimates and the establishment of the local temperature-density relationship to be able to compute such estimates from the moored temperature observations.

Moored temperature observations are transferred to conservative temperature Θ [*McDougall et al.*, 2009], before they are used as a proxy for potential density anomalies referenced to 3000 dbar ($\delta\sigma_{3000}$): $\delta\sigma_{3000} = \alpha\delta\Theta$, where $\alpha = -0.06 \pm 0.005$ kg m^{-3}°C^{-1} and $\alpha = -0.07 \pm 0.005$ kg m^{-3}°C^{-1} are the apparent thermal expansion coefficients under local conditions, for 2500–3000 and 2200 m, respectively. These relationships are the mean for the lower 400 m above the bottom of the CTD profiles. Turbulent kinetic energy dissipation rate ε (and vertical eddy diffusivity K_z) is estimated via a classic oceanographic method [*Thorpe,* 1977, 1987], calculating "overturn displacements" d after sorting every 1 Hz potential density profile, which may contain unstable inversions, into a stable monotonic profile without inversions. A threshold of 3×10^{-6} kg m^{-3} is applied to disregard apparent displacements associated with remaining temperature shifts after calibration [*van Haren et al.*, 2009]. This threshold is the same for all data sets. After comparing d with the Ozmidov scale [*Dillon*, 1982], $\varepsilon = 0.64 d^2 N^3$. In weak stratification ($N \approx f$), the threshold limits resolution of ε to O(10^{-12}) W kg^{-1}. Similarly, $K_z = \Gamma \varepsilon N^{-2}$ using a mixing efficiency for the conversion of kinetic into potential energy of $\Gamma = 0.2$ and which is typical for shear-induced turbulence [*Osborn*, 1980; *Oakey*, 1982]. We note that constant Γ is for high Reynolds number (10^4–10^6) flows as is typical for both estuarine conditions [*Geyer et al.*, 2010] and above deep-ocean topography [*van Haren and Gostiaux*, 2012] where rapid restratification is observed.

Acknowledgments

Captain and crew of R/V *Pelagia* are acknowledged for mooring deployment and recovery. We greatly thank M. Laan for design and construction of NIOZ temperature sensors and his and MTM's assistance in mooring preparation. We thank H. de Haas for working up the Multibeam data and preparing Figure 1. L. Gerringa critically reviewed an earlier draft. Data use requests can be directed to hans.van.haren@nioz.nl.

The Editor thanks an anonymous reviewer for their assistance in evaluating this paper.

References

Armi, L. (1979), Effects of variations in eddy diffusivity on property distributions in the oceans, *J. Mar. Res.*, *37*, 515–530.

Bonnin, J., H. van Haren, G.-J. Brummer, and P. Hosegood (2006), Burst resuspension of seabed material at the foot of the continental slope in the Rockall Channel, *Mar. Geol.*, *226*, 167–184.

Cacchione, D. A., and D. E. Drake (1986), Nepheloid layers and internal waves over continental shelves and slopes, *Geo Mar. Lett.*, *16*, 147–152.

Dickson, R. R., and I. N. McCave (1986), Nepheloid layers on the continental slope west of Porcupine Bank, *Deep Sea Res., Part I*, *33*, 791–818.

Dillon, T. M. (1982), Vertical overturns: A comparison of Thorpe and Ozmidov length scales, *J. Geophys. Res.*, *87*, 9601–9613, doi:10.1029/JC087iC12p09601.

Ekman, V. W. (1905), On the influence of the Earth's rotation on ocean-currents, *Ark. Math. Astron. Fys.*, *2*(11), 1–52.

Eriksen, C. C. (1982), Observations of internal wave reflection off sloping bottoms, *J. Geophys. Res.*, *87*, 525–538, doi:10.1029/JC087iC01p00525.

Garrett, C. (1990), The role of secondary circulation in boundary mixing, *J. Geophys. Res.*, *95*, 3181–3188, doi:10.1029/JC095iC03p03181.

Geyer, W. R., A. C. Lavery, M. E. Scully, and J. H. Trowbridge (2010), Mixing by shear instability at high Reynolds number, *Geophys. Res. Lett.*, *37*, L22607, doi:10.1029/2010GL045272.

Gonella, J., and D. Michon (1988), Ondes internes profondes révélées pas sismique reflexion au sein des masses d'eau en Atlantique-Est, *C. R. Acad. Sci. Paris*, *306*, 781–787.

Gregg, M. C. (1989), Scaling turbulent dissipation in the thermocline, *J. Geophys. Res.*, *94*, 9686–9698, doi:10.1029/JC094iC07p09686.

Hosegood, P., J. Bonnin, and H. van Haren (2004), Solibore-induced sediment resuspension in the Faeroe-Shetland Channel, *Geophys. Res. Lett.*, *31*, L09301, doi:10.1029/2004GL019544.

Iwamae, N., and T. Hibiya (2012), Numerical study of tide-induced mixing over rough bathymetry in the abyssal ocean, *J. Oceanogr.*, *68*, 195–203.

Klymak, J. M., R. Pinkel, and L. Rainville (2008), Direct breaking of the internal tide near topography: Kaena Ridge, Hawaii, *J. Phys. Oceanogr.*, *38*, 380–399.

Klymak, J. M., S. Legg, and R. Pinkel (2010), A simple parameterization of turbulent mixing near supercritical topography, *J. Phys. Oceanogr.*, *40*, 2059–2073.

Legg, S., and A. Adcroft (2003), Internal wave breaking at concave and convex continental slopes, *J. Phys. Oceanogr.*, *33*, 2224–2246.
McDougall, T. J., et al. (2009), Calculation of the thermodynamic properties of seawater, global ship-based repeat hydrography manual, *IOCCP Rep. 14, ICPO Publ. Ser., 134*, U.N.E.S.C.O., Paris.
Munk, W. (1966), Abyssal recipes, *Deep Sea Res.*, *13*, 707–730.
Munk, W., and C. Wunsch (1998), Abyssal recipes II: Energetics of tidal and wind mixing, *Deep Sea Res., Part I*, *45*, 1977–2010.
Nash, J. D., M. H. Alford, E. Kunze, K. Martini, and S. Kelly (2007), Hotspots of deep ocean mixing on the Oregon continental slope, *Geophys. Res. Lett.*, *34*, L01605, doi:10.1029/2006GL028170.
Nikurashin, M., and S. Legg (2011), A mechanism for local dissipation of internal tides generated at rough topography, *J. Phys. Oceanogr.*, *41*, 378–395.
Oakey, N. S. (1982), Determination of the rate of dissipation of turbulent energy from simultaneous temperature and velocity shear microstructure measurements, *J. Phys. Oceanogr.*, *12*, 256–271.
Orlanski, I., and K. Bryan (1969), Formation of thermocline step structure by large-amplitude internal gravity waves, *J. Geophys. Res.*, *74*, 6975–6983, doi:10.1029/JC074i028p06975.
Osborn, T. R. (1980), Estimates of the local rate of vertical diffusion from dissipation measurements, *J. Phys. Oceanogr.*, *10*, 83–89.
Thorpe, S. A. (1977), Turbulence and mixing in a Scottish loch, *Phil. Trans. R. Soc. Lond. A*, *286*, 125–181.
Thorpe, S. A. (1987), Current and temperature variability on the continental slope, *Phil. Trans. R. Soc. Lond. A*, *323*, 471–517.
Thorpe, S. A. (1988), Benthic boundary layers on slopes, in *Small Scale Turbulence and Mixing in the Ocean, Proc. 19th Int. Liège Colloq. On Hydrodynamics*, edited by J. C. J. Nihoul and B. M. Jamart, pp. 425–433, Elsevier, Amsterdam.
van Haren, H. (2005), Details of stratification in a sloping bottom boundary layer of Great Meteor Seamount, *Geophys. Res. Lett.*, *32*, L07606, doi:10.1029/2004GL022298.
van Haren, H., and L. Gostiaux (2012), Detailed internal wave mixing observed above a deep-ocean slope, *J. Mar. Res.*, *70*, 173–197.
van Haren, H., M. Laan, D.-J. Buijsman, L. Gostiaux, M. G. Smit, and E. Keijzer (2009), NIOZ3: Independent temperature sensors sampling yearlong data at a rate of 1 Hz, *IEEE J. Ocean. Eng.*, *34*, 315–322.
van Haren, H., L. R. M. Maas, and T. Gerkema (2010), Patchiness in internal tidal beams, *J. Mar. Res.*, *68*, 237–257.
van Raaphorst, W., H. Malschaert, H. van Haren, W. Boer, and G.-J. Brummer (2001), Across-slope zonation of erosion and deposition in the Faeroe-Shetland Channel, *Deep Sea Res., Part I*, *48*, 567–591.